Microsc. Microanal. 15, 125–129, 2009
doi:10.1017/S1431927609090205

Microscopy AND Microanalysis

Secondary Electron Emission Contrast of Quantum Wells in GaAs p-i-n Junctions

Enrique Grunbaum,[1,*] Zahava Barkay,[2] Yoram Shapira,[1] Keith W.J. Barnham,[3] David B. Bushnell,[3] Nicholas J. Ekins-Daukes,[3] Massimo Mazzer,[3] and Peter Wilshaw[4]

[1]*Department of Physical Electronics, Faculty of Engineering, Tel-Aviv University, Tel-Aviv 69978, Israel*
[2]*Wolfson Applied Materials Research Centre, Tel-Aviv University, Tel-Aviv 69978, Israel*
[3]*Department of Physics, Imperial College of Science, Technology & Medicine, London SW7 2BW, UK*
[4]*Department of Materials, Parks Road, University of Oxford, Oxford OK1 3PH, UK*

Abstract: The secondary electron (SE) signal over a cleaved surface of GaAs p-i-n solar cells containing stacks of quantum wells (QWs) is analyzed by high-resolution scanning electron microscopy. The InGaAs QWs appear darker than the GaAsP barriers, which is attributed to the differences in electron affinity. This method is shown to be a powerful tool for profiling the conduction band minimum across junctions and interfaces with nanometer resolution. The intrinsic region is shown to be pinned to the Fermi level. Additional SE contrast mechanisms are discussed in relation to the dopant regions themselves as well as the AlGaAs window at the p-region. A novel method of *in situ* observation of the SE profile changes resulting from reverse biasing these structures shows that the built-in potential may be deduced. The obtained value of 0.7 eV is lower than the conventional bulk value due to surface effects.

Key words: high-resolution scanning electron microscopy, secondary electrons, quantum wells, conductance band, valence band, dopant contrast, GaAs

Introduction

The variation in the secondary electron (SE) emission in a high-resolution scanning electron microscope (HRSEM) of n-p or n-i-p semiconductor devices has been shown to reflect the dopant type and concentration in the various structure regions (Perovic et al., 1995; Venables et al., 1998; Sealy et al., 2000; Elliott et al., 2002; Barkay et al., 2003, 2005; Castelli et al., 2003; El-Gomati et al., 2005). This effect was explained by the differences in SE emission due to the differences in ionization energy of the different regions (Sealy et al., 2000). The ionization energy is defined as the energy required to move an electron from the top of the valence band to a position at the detector far away (several hundred micrometers according to Buzzo et al., 2006); the difference in this energy from one side of the junction to the other is of the order of half the built-in potential that is present across the junction. It justifies the observations of p-doped layers appearing brighter than n-doped region (first observed by Chang & Nixon, 1967).

Efforts have been made to obtain quantitative values of the dopant concentration. A linear relationship between the observed contrast and the logarithm of the dopant concentration has been found for the dopant concentration in p-type Si in the range of 10^{16} and 10^{20} cm^{-3} (Venables et al., 1998). More recently, using energy filtering in the SE imaging, an accuracy of ±8.5% was obtained in the quantification of dopant concentration in Si in the 2.8×10^{17}–7.5×10^{19} cm^{-3} (Schonjahn et al., 2002; Kazemian et al., 2006). The contributions of different mechanisms for the SE contrast—(1) material composition, (2) dopant concentration, (3) built-in potential, and (4) external applied bias—have been demonstrated and discussed. The influence of carbon contamination and other layers on the SE contrast has also been studied (El-Gomati et al., 2005).

The difference in ionization energy as a function of doping is equal to the difference in electron affinity for junctions of the same band gap. However, multiple-quantum wells (MQWs), which are discussed in this work, provide a different situation, according to which the band gap varies across the junction. In this work we present new experimental data from a solar cell based on an MQW p-i-n structure. The results show that the contrast profile of a line scan across the MQW delineates the conduction band minimum (CBM) of the structure. This new interpretation, which may be denoted as "electron affinity contrast," is shown to be a powerful tool for CBM profiling. The profiling technique provides essential information on the electronic structure across semiconductor junctions and interfaces with nanometer resolution.

Received January 15, 2008; accepted February 20, 2008
*Corresponding author. E-mail: enrique@eng.tau.ac.il

Table 1. Layer Layout Samples QT1410R (20 QWs) and QT1629 (10 QWs).

		Sample			
		QT1410R (20 QWs)		QT1629 (10 QWs)	
Layer	Doping (cm^{-3})	Thickness (nm)		Thickness (nm)	
GaAs	Zn p^+ 3×10^{19}	1,000		220	
$Al_{0.8}Ga_{0.2}As$	C $p > 5 \times 10^{18}$	43		43	
GaAs	C $p\ 5 \times 10^{18}$	200×2		400	
GaAs buffer		**10**		**60**	
$GaAs_{0.91}P_{0.09}$ barriers	Intrinsic	**22.7×20**	**1,088**	**9.3×10**	**386**
$In_{0.15}Ga_{0.85}As$ QWs		**8×20**		**8×10**	
$GaAs_{0.91}P_{0.09}$ barriers		**22.7×20**		**9.3×10**	
GaAs buffer		**10**		**60**	
GaAs	Si n 1.5×10^{18}	3,000		2,000	
GaAs	Si n 1.5×10^{18}	300		300	
GaAs substrate	n^+				

Materials and Methods

The quantum well solar cells (QWSCs; Barnham et al., 2000, 2002) consisted of III-V compound layers (such as GaAs) doped to form a p-i-n structure and a number of thin-layer QWs of another III-V compound (such as InGaAs) with a lower band gap. These layers are inserted into the intrinsic (i) region, thus forming a stack of periodic-barrier quantum wells. In this work, we show that the nanosize (8 or 11 nm wide) quantum wells can be distinguished and their type of contrast determined using HRSEM. QWSC devices consisting of p-i-n GaAs junctions having strain-balanced $In_{0.15}GaAs/GaAsP_{0.09}$ MQW structures in the intrinsic region (Ekins-Daukes et al., 1999) were epitaxially grown by metal-organic vapor deposition at the National Centre for III-V Technologies at Sheffield University, UK. The layout of the layers for two different types of samples: QT 1410R and QT 1629 with 20 and 10 QWs, respectively, is given in Table 1. Cross sections were prepared by cleavage of the sample at the (110) plane in air immediately prior to the measurements. A uniform adsorbed layer at the cleaved surface should be expected but should not alter the conclusions. To eliminate the intensive contamination inside the HRSEM, which is usually observed with successive scans of the same position, the bias variations were done within the same scan, using a specially designed voltage kit. In addition, a cold trap helped in reducing the surface contamination during imaging.

A cold field emission HRSEM (JEOL 6700F) was used, combined with a semi-in lens SE detector, which provides efficient collection, allowing observation of nanometer scale features. The efficient collection of the SEs was obtained by the semi-in lens detector arrangement, consisting of three apertures to which biases were applied to extract and deflect the SEs toward the detector. Observations are made with a primary energy of 2 keV and a primary beam current of 100 pA.

Results and Discussion

Quantum Well SE Contrast

The SE line scans in the HRSEM of samples QT 1410R and QT1629 (Figs. 1, 2) show clearly the contrast from the QWs in the intrinsic (i) region. The SE signal is displayed by scanning the incident beam from left to right and averaging over a selected area. The 8-nm-wide QWs are well resolved and appear darker than the adjacent 46-nm or 19-nm-wide barriers regions (see Table 1). Hence, the QWs correspond to minima in the SE profiles. The observed contrast is discussed in terms of electron-hole (e-h) generation by the primary beam and SE emission mechanisms. The e-h generated current (N) by the primary beam is given approximately (Reimer, 1985) by

$$N = \frac{E_P}{E_i} \cdot (1 - \eta) \cdot I_P, \tag{1}$$

where E_P is the primary beam energy, I_P is the primary beam current, η is the backscattering coefficient, and E_i is the mean e-h excitation energy, which is given by $2 \cdot E_g + 1.3$ (eV), where E_g is the energy gap.

The e-h generation is thus similar within 10% for the $In_{0.15}GaAs$ and the $GaAsP_{0.09}$ regions in the QW/barrier structure (band gap of 1.18 and 1.47 eV, respectively). However, the SE emission, which depends on the affinity, plays a major role in the observed contrast. The band diagram with the CBM and the affinities χ_{QW} and χ_B,

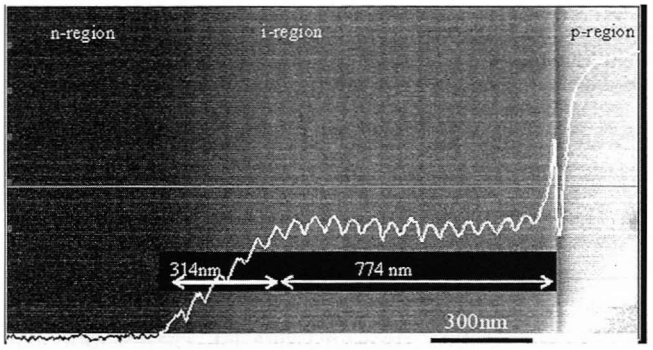

Figure 1. HRSEM image at 2 keV and line scan of SE signal (averaged the marked area) of sample QT1410RC with 20QWs (layout in Table 1).

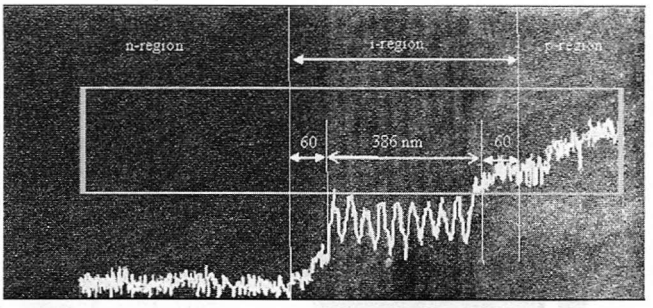

Figure 2. HRSEM image at 2 keV with line scan of SE signal (averaged over the marked area) of sample QT1629 with 10QWs (layout in Table 1).

which correspond to the emission energy of the secondary electrons from the QWs and barriers, respectively, is shown in Figure 3. The CBM of the QWs is 0.29 eV lower than that of the adjacent GaAs barrier layers, which did result in relatively lower SE emission at the QW.

A comparative study of the same sample QT1410R by Kelvin probe force microscopy operating in an ultrahigh vacuum system was performed previously (Schwarzman et al., 2005). There the contact potential difference measurement, i.e., the electron affinity determination, provided direct information on the surface potential distribution.

The i-Region SE Contrast

A dominant feature in Figures 1 and 2 is the large increase in SE beginning at the physical interface of the n-region with the i-region. It extends into the latter by 314 nm and 60 nm, respectively. This corresponds to the depletion region of a one-sided abrupt electrical n-p junction (Sze, 1981). This strong electric field in the intrinsic region is followed by a weak electric field extending through the remaining intrinsic region, as seen in Figures 1 and 2 as a nearly horizontal contrast line (774 nm and 386 nm), where most of the QWs are located. It should be noted that a certain number of QWs falls into the strong field i-regions (see Figs. 1, 2). This depends only on the layer layout of the QWs in the particular sample type.

This main part of the i-region has the character of a weakly doped p-region (1×10^{15} cm^{-3}), due to unwanted impurities. The measured quantum efficiency of the solar cell points to the existence of a weak field in this region; it is drawn in Figure 3 as a slightly upward slanted line (Barnham et al., 2000, 2002). However, the observed nearly horizontal SE contrast line is attributed to the fact that the location of this part of the i-region coincides with that of the Fermi level. This pinning of the i-region is due to surface states present in the semiconductor. They strongly influence the emission of the SEs, which are emitted close to the specimen surface.

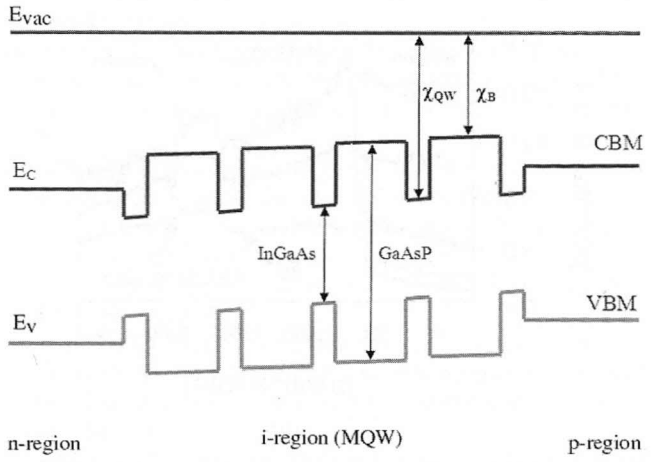

Figure 3. Band diagram showing the conductance band minimum CBM and the affinity χ of the QWs, and of the barriers, respectively; these determine the QW contrast.

Dopant and Window SE Contrast

The n-region shows a low SE intensity level relative to the p-region (Figs. 1, 2). Beyond the (low p-doped) i-region, their contrast is steadily increasing toward the p+ region. This is attributed to the gradually decreasing influence of the surface states.

The contrast between the n- and p-regions was explained by the difference in ionization energy of the different regions (Sealy et al., 2000 and the introduction to this article); its value is given by the built-in potential (Barkay et al., 2003).

The 43-nm-wide intrinsic $Al_{0.8}Ga_{0.2}As$ window inserted between the two p-layers (Table 1) shows a dip in the SE signal intensity (Fig. 4a,b). This contrast is explained by backscattering-induced SE, i.e., due to lower backscattered electron contribution to the SE signal at the AlGaAs region ($\eta = 0.315$) relative to the GaAs region ($\eta = 0.358$) as shown in Table 2. The η values in Table 2 are calculated according to the traditionally accepted mass fraction method for the

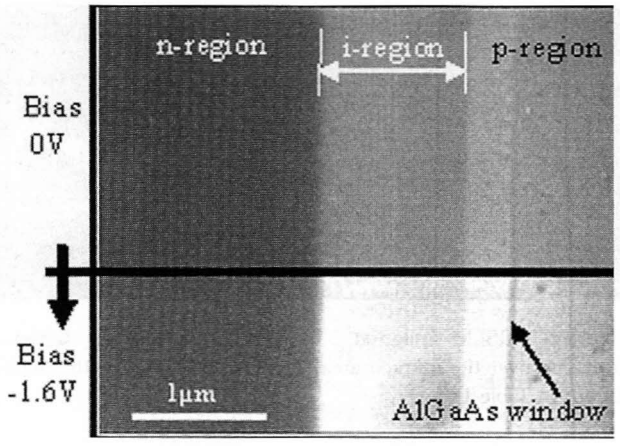

(a)

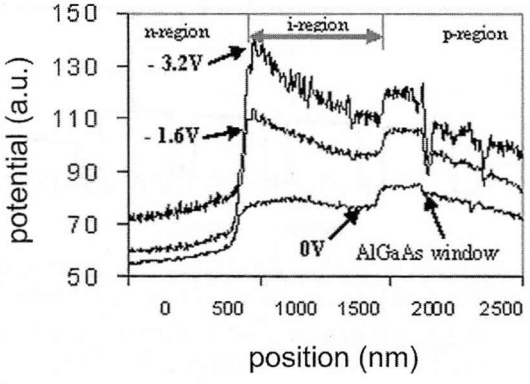

(b)

Figure 4. HRSEM images at 2 keV with line scan of sample QT1410R: (**a**) bias change from 0 to −1.6 V during image scan for recording; (**b**) graph showing the three corresponding line scans of SE signal, obtained with applied biases of 0, −1.6, and −3.2 V.

multicomponent materials (Castaing, 1960; Goldstein et al., 2003). The element values at low beam energy correspond to the material database for electron-solid interactions (Joy, 2008). For comparison, according to Table 2, the backscattered effect is minimal for $In_{0.15}Ga_{0.85}As/GaAs_{0.91}P_{0.09}$ (when $\eta = 0.362$ for $In_{0.15}Ga_{0.85}As$ and $\eta = 0.355$ for $GaAs_{0.91}P_{0.09}$). The QW/barrier SE contrast thus rather follows the CBM description as previously discussed.

Application of a Reverse Bias and Determination of the Inner Potential

The n-i junction built-in potential is calibrated by applying an external reverse bias *in situ* using a specially designed voltage kit, with the substrate being grounded and the voltage being applied to the surface layer. This compact kit is suitable whenever inserting a sample into the HRSEM using an airlock (as is the present case) and is designed so that its upper level fits the sample cross-section surface,

Table 2. Calculated Backscattering Coefficient η of Multicomponent Materials for $E_p = 2$ keV.

Material	η ($E_p = 2$ keV)
GaAs	0.358
$In_{0.15}Ga_{0.85}As$	0.362
$GaAs_{0.91}P_{0.09}$	0.355
$Al_{0.8}Ga_{0.2}As$	0.315

providing SE emission from the specimen in close vicinity to the SE detector. The kit, together with the studied sample, is inserted into the vacuum specimen chamber providing periodic *in situ* biasing with predetermined values, while imaging the sample using the SE detector. The predetermined biasing ramp rate helps to observe and record the bias-induced SE changes during a single image scan; this allows the contrast comparison of images having similar concentration of unwanted carbon contamination.

HRSEM micrographs of sample QT1410R (20 QWs), with and without applying a reverse bias of −1.6 V, are shown in Figure 4a. The abrupt voltage change from 0 to −1.6 V was preprogrammed to occur in the middle of the image scan (Fig. 4a). The corresponding SE intensity curves for 0, −1.6, and −3.2 V are plotted in Figure 4b. The enhancement of the SE signal, which is observed in the i region, is attributed to the increased electron accumulation at the n-i interface and is explained by enhanced e-h separation at the intrinsic region under external biasing.

The displacement of the p-n levels due to the −1.6-V reverse bias is used as a calibration of the SE scan lines. From the difference, the value of 0.7 V is deduced for the built-in potential. This is much lower than the value of 1.1 V measured previously in strained GaAs well samples (Barnes et al., 1996); Similar differences have been measured in Si samples and justified by modeling (Elliott et al., 2002; Kazemian et al., 2006; Chee et al., 2007). This phenomenon is due to presence in the i-region of surface states, as explained above.

Conclusions

The contribution of a few types of SE mechanisms to SE emission is discussed, based on p-i(MQW)-n solar cells and using quantitative HRSEM. The technique demonstrates (1) nanoscale resolution, (2) composition sensitivity, (3) sensitivity to dopant concentration and type, (4) sensitivity to external reverse bias, and (5) possibility to deduce the built-in potential. In particular, the HRSEM analysis provides an excellent noncontact method for describing the CBM of semiconductor structures at nanometer resolution. Additional practical applications are the precise measurement of

the dimensions of the various regions and features and their comparison with the designer specifications. Furthermore, the application of an external bias enhances the distinction between these regions and particular features.

Acknowledgments

We acknowledge the cooperation of Ezra Shaked of the School of Physics, Tel-Aviv University, with the skillful design of the electronic circuit for the periodic *in situ* biasing of the specimen. Y.S. is grateful to Monash University, Melbourne, Australia for hosting him during his sabbatical.

References

Barkay, Z., Grunbaum, E., Shapira, Y., Wilshaw, P., Barnham, K., Bushnell, D.B., Ekins-Daukes, N.J. & Mazzer, M. (2003). High-resolution scanning electron microscopy of dopants in p-i-n junctions with quantum wells. *Inst Phys Conf Ser* **179**, 143–146.

Barkay, Z., Grunbaum, E., Shapira, Y., Wilshaw, P., Barnham, K., Bushnell, D.B., Ekins-Daukes, N.J. & Mazzer, M. (2005). The electric field and dopant distribution in p-i-n structures observe by ionization potential (dopant contrast) microscopy in the HRSEM. *Proc Microscopy of Semiconducting Materials XIV*, Oxford, UK, Cullis, A.G. & Hutchison, J.L. (Eds.), pp. 503–506. Berlin: Springer Press.

Barnes, J., Nelson, J., Barnham, K.W.J., Roberts, J.S., Pate, M.A., Grey, R., Dosanjh, S.S., Mazzer, M. & Ghiraldo, F. (1996). Characterization of GaAs/InGaAs quantum wells using photocurrent spectroscopy. *J Appl Phys* **79**, 7775–7779.

Barnham, K.W.J., Ballard, I., Connolly, J.P., Ekins-Daukes, N.J., Kluftinger, B.G., Nelson, J. & Rohr, C. (2002). Quantum well solar cells. *Physica* **14**, 27–36.

Barnham, K.W.J., Ballard, I., Connolly, J.P., Ekins-Daukes, N.J., Kluftinger, B.G., Nelson, J., Rohr, C. & Mazzer, M. (2000). Recent results on quantum well solar cells. *J Mater Sci Mater Electron* **11**, 531–536.

Buzzo, M., Ciappa, M. & Fichtner, W. (2006). Imaging and dopant profiling of silicon carbide devices by secondary electron dopant contrast. *IEEE Trans Device Mater Reliab* **6**, 203–212.

Castaing, R. (1960). Electron probe microanalysis. *Adv Electron El Phys* **13**, 317–386.

Castelli, R.M., Muller, D.A. & Voyles, P.M. (2003). Dopant mapping for the nanotechnology age. *Nat Mater* **2**, 129–131.

Chang, T.H.P. & Nixon, W.C. (1967). Electron beam induced potential contrast on unbiased planar transistors. *Solid State Electr* **10**, 701–704.

Chee, K.W.A., Rodenburg, C. & Humphreys, C.J. (2007). Quantitative dopant profiling in SEM. *Proc Microscopy of Semiconducting Materials XV Conf*, Cambridge, UK, Cullis, A.G. & Midgley, P.M. (Eds.), pp. 407–410. Berlin: Springer Press.

Ekins-Daukes, N.J., Barnham, K.W.J., Connolly, J.P., Roberts, J.S., Clark, J.C., Hill, G. & Mazzer, M. (1999). Strain-balanced GaAsP/InGaAs quantum well solar cells. *Appl Phys Lett* **75**, 4195–4197.

El-Gomati, M., Zaggout, F., Jayacody, H., Tear, S. & Wilson, K. (2005). Why is it possible to detect doped regions of semiconductors in low voltage SEM: A review and update. *Surf Interface Anal* **37**, 901–911.

Elliott, S.L., Broom, R.F. & Humphreys, C.J. (2002). Dopant profiling with the scanning microscope—A study of Si. *J Appl Phys* **91**, 9116–9122.

Goldstein, J., Newbury, D., Joy, D., Lyman, C., Echlin, P., Lifshin, E., Sawyer, L. & Michael, J. (2003). *Scanning Electron Microscopy and X-ray Microanalysis*. New York: Plenum Press.

Joy, D.C. (2008). A database for electron solid interactions. Available at http://web.utk.edu/~srcutk/database.doc.

Kazemian, P., Mentink, S.A.M., Rodenburg, C. & Humphreys, C.J. (2006). High resolution quantitative two-dimensional mapping using energy-filtered secondary electron imaging. *J Appl Phys* **100**, 054901-7.

Perovic, D.D., Castell, M.R., Howie, A., Lavoie, C., Tiedje, T. & Cole, J.S.W. (1995). Field-emission SEM imaging of compositional and doping layer semiconductor superlattices. *Ultramicroscopy* **58**, 104–113.

Reimer, L. (1985). *Scanning Electron Microscopy: Physics of Image Formation and Microanalysis*. Berlin: Springer Verlag Press.

Schonjahn, C., Humphreys, C.J. & Glick, M. (2002). Energy-filtered imaging in a field-emission scanning electron microscope for dopant mapping in semiconductors. *J Appl Phys* **92**, 7667–7671.

Schwarzman, A., Grunbaum, E., Strassburg, E., Lepkifker, E., Boag, A. & Rosenwaks, Y. (2005). Nanoscale potential distribution across multi-quantum well structures: Kelvin probe force microscopy and secondary electron imaging. *J Appl Phys* **98**, 084310-1-4.

Sealy, C.P., Castell, M.R. & Wilshaw, P.R. (2000). Mechanism for secondary electron dopant contrast in the SEM. *J Electron Microsc* **49**, 311–321.

Sze, S.M. (1981). *Physics of Semiconductor Devices*, 2nd ed. New York: John Wiley.

Venables, D., Jain, H. & Collins, D.C. (1998). Secondary electron imaging as a two-dimensional dopant profiling technique: Review and update. *J Vac Sci Technol B* **16**, 362–366.